Spherical Pendulum, Actions, and Spin

Richter, Peter H.; Dullin, Holger R.; Waalkens, Holger; Wiersig, Jan

Published in:
The Journal of Physical Chemistry

Publication date:
1996

Spherical Pendulum, Actions, and Spin†

Peter H. Richter,*,‡ Holger R. Dullin, Holger Waalkens, and Jan Wiersig

Institut für Theoretische Physik and Institut für Dynamische Systeme, University of Bremen, Postfach 330 440, D-28334 Bremen, Germany

Received: June 11, 1996⊗

The classical and quantum mechanics of a spherical pendulum are worked out, including the dynamics of a suspending frame with moment of inertia θ. The presence of two separatrices in the bifurcation diagram of the energy−momentum mapping has its mathematical expression in the hyperelliptic nature of the problem. Nevertheless, numerical computation allows to obtain the action variable representation of energy surfaces and to derive frequencies and winding ratios from there. The quantum mechanics is also best understood in terms of these actions. The limit $\theta \rightarrow 0$ is of particular interest, both classically and quantum mechanically, as it generates two copies of the frameless standard spherical pendulum. This is suggested as a classical interpretation of spin.

1. Introduction

John Ross was born in the year when Schrödinger's equation and Born's statistical interpretation of the wave function were published. The triumph of quantum theory left only minor roles for classical mechanics, in the exciting game of exploring the microscopic world of atomic and molecular dynamics. The year before, with Born's publication of his *Vorlesungen über Atommechanik*,[1] the old Bohr−Sommerfeld idea to understand energy spectra on the basis of discretizing classical action integrals in multiples of $\hbar$ had reached its culmination point, and at the same time come to a dead end. Friedrich Hund, who contributed substantial parts to that book, confessed many years later that in the Göttingen theoretical physical seminar they had tried hard to make use of Poincaré's new methods for dealing with nonintegrable mechanical systems, but as Einstein had clearly foreseen in 1917,[2] the quantum theorists of old could not absorb them in their concepts; as a result, the matter was dropped and left out of Born's book. In contrast, Heisenberg's and Schrödinger's new quantum mechanics did not suffer from this difficulty: integrability was not an issue, at least so it seemed. Separable or not, the Schrödinger equation could be written down and solved, if only in principle. Poincaré became forgotten in the physics community.

Things changed when *chaos* was (re)discovered, about 50 years later. The combined impact of beautiful mathematical results as in the Kolmogorov−Arnold−Moser theory, and of the computer revolution, renewed the interest first in classical mechanics, then in the quantum mechanics of nonseparable systems. The term *quantum chaology* was coined to refer to the specific features of quantum systems whose classical counterpart is nonintegrable.[3,4] So far, the major achievement in this field of research has been the discovery that action integrals along classical periodic orbits are the key to understanding complicated spectra.[5]

In light of this development, the interest in the computation of actions has been revived. Screening through the literature, one finds surprisingly little concrete knowledge for nontrivial systems, even though textbooks and review articles[6,7] stress their general importance for perturbation theory and quantization. To fill this gap, our research group has worked out energy surfaces in action variable representation, for a number of classical problems: the Euler, Lagrange, and Kovalevskaya cases of rigid body dynamics,[8−10] billiards in ellipsoids,[11,12] and particle motion around point masses with Schwarzschild or Kerr metric as well as around two fixed centers.[13] The typical shape of these surfaces, for systems with three degrees of freedom, has turned out to be a pyramid of some sort.

In the course of these studies we considered rigid bodies with Cardan suspensions. The configuration space of such systems is a 3-torus T^3, as three angular coordinates may vary independently along a full circle. This is an essential distinction to the configuration space SO(3) of an isolated rigid body where one of the three Euler angles varies only from 0 to π. It is common thinking among physicists that pure SO(3) dynamics emerges in the limit where the moments of inertia of the Cardan frames vanish, but how should the transition from T^3 to SO(3) in configuration space be described? In a forthcoming monograph,[14] we propose to consider T^3 as a double cover of SO(3) and to understand the limit as a transition from T^3 to *two* copies of SO(3). In a natural way, this point of view introduces a classical spin variable for distinction between the two copies.

The same reasoning is applied in the present paper to the spherical pendulum and is carried over from classical to quantum mechanics. The configuration space of the isolated spherical pendulum is the sphere S^2; with suspension it becomes a 2-torus T^2. Whereas the isolated system is always integrable, the suspension frame may spoil the integrability, but we shall concentrate on the case where both systems have a conserved angular momentum L_φ. The energy surfaces are then foliated by invariant Liouville tori and may be transformed to action variable representation. We determine the bifurcation scheme of critical tori and the classical action integrals. As long as the moment of inertia of the frame θ does not vanish, there exists a system of separatrices which defines three types of motion, or "phases", two of which appear in two copies due to spontaneous symmetry breaking. One of these two types corresponds to the motion of the pure spherical pendulum. It is the only phase to survive in the limit $\theta \rightarrow 0$; its two copies may be assigned a classical spin.

The quantum mechanical spectrum is determined both numerically and in semiclassical approximation. The agreement is almost perfect and demonstrates how remarkably powerful the recipes of old quantum theory are, if combined with simple rules to account for symmetry and topology of classical tori as

† Dedicated to John Ross on the occasion of his 70th birthday.

‡ E-mail: prichter@physik.uni-bremen.de.

⊗ Abstract published in *Advance ACS Abstracts,* November 1, 1996.

S0022-3654(96)01712-1 CCC: $12.00

well as for smooth transitions across separatrices. As in the classical treatment, the $\theta \to 0$ limit produces the pure spherical pendulum physics with twofold degeneracy.

The organization of the paper is as follows. Section 2 defines the classical Hamiltonians, first of the pure spherical pendulum and then with suspending frame. The foliation of phase space by invariant tori, and its bifurcation scheme, is discussed in section 3. The classical analysis is completed in section 4 where we calculate action integrals, energy surfaces, and frequencies. We show how the limit $\theta \to 0$ produces two copies of the pure spherical pendulum, with opposite spin. Finally, section 5 presents the quantum mechanical spectrum, first in terms of energy and angular momentum eigenvalues and then in the more transparent action eigenvalue representation.

2. Isolated and Suspended Spherical Pendulum

The mathematical definition of a spherical pendulum assumes a mass point m, free to move on a sphere S^2 of radius r, in an external gravitational potential that depends linearly on a coordinate z. Using spherical coordinates (φ,ϑ) to parametrize the configuration space $Q = S^2$ by longitude $\varphi \in S^1$ and latitude ϑ, ranging from $\vartheta = 0$ at the north pole to $\vartheta = \pi$ at the south pole ($z = \cos\vartheta$), kinetic energy T and potential energy V are

$$T = {}^1\!/_2 mr^2 (\dot\vartheta^2 + \dot\varphi^2 \sin^2\vartheta), \quad V = mgr(1 + \cos\vartheta) \quad (1)$$

The potential minimum $V = 0$ occurs at the south pole. Measuring energies in units of mgr, times in units of $\sqrt{r/g}$, hence actions in units of $mr\sqrt{gr}$, the dimensionless Lagrangian is

$$L = {}^1\!/_2\dot\vartheta^2 + {}^1\!/_2\dot\varphi^2 \sin^2\vartheta - 1 - \cos\vartheta \quad (2)$$

With $L_\vartheta = \dot\vartheta$ and $L_\varphi = \dot\varphi \sin^2\vartheta$ as the angular momenta, the corresponding Hamiltonian becomes

$$H = {}^1\!/_2 L_\vartheta^2 + {}^1\!/_2 \frac{L_\varphi^{\,2}}{\sin^2\vartheta} + 1 + \cos\vartheta \quad (3)$$

In a physical implementation of this system, a device must be chosen to hold the mass point on the sphere. It is practically impossible to do this without changing the dynamics in an essential way. On the one hand, there are moving parts in addition to the mass m, implying new terms in the equations of motion. On the other hand, and more severely, the enlarged total system almost inevitably (we leave it as a challenge to the reader to name a counterexample; perhaps we are too prejudiced to find any) has a configuration space different from S^2. This poses the interesting problem as to how the pure spherical pendulum may be recovered in a physical limit of some kind.

Consider Figure 1 as a possible and fairly typical realization. It derives from a Cardan suspension for rigid body motion whose third axis is not used here for rotation but only carries the mass point m. The angle φ describes the position of the frame F to which the (massless) ϑ-axis is firmly attached. The energy contributions of the mass m are the same as in eq 1, but in addition there is a kinetic energy $T^F = {}^1\!/_2\theta^F\dot\varphi^2$ associated with the motion of the frame, θ^F being its moment of inertia. With the same scaling as before, and using $\theta = \theta^F/mr^2$ as a dimensionless parameter to characterize the frame, the Lagrangian reads

$$L = {}^1\!/_2\dot\vartheta^2 + {}^1\!/_2(\theta + \sin^2\vartheta)\dot\varphi^2 - 1 - \cos\vartheta \quad (4)$$

The angular momenta are $L_\vartheta = \dot\vartheta$ and $L_\varphi = (\theta + \sin^2\vartheta)\,\dot\varphi$,

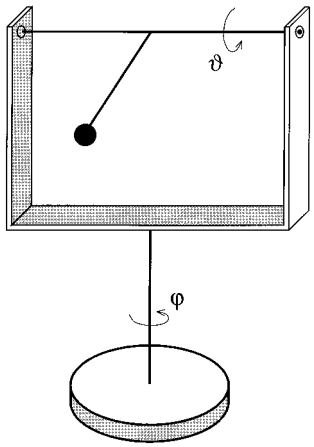

Figure 1. Spherical pendulum suspended in a frame F. The frame rotates here about a vertical axis; its position is given by the angle of longitude φ. The horizontal ϑ-axis is fixed in F. The mass point m is rigidly connected to this axis by a massless rod.

and the Hamiltonian

$$H = {}^1\!/_2 L_\vartheta^{\,2} + {}^1\!/_2 \frac{L_\varphi^{\,2}}{\theta + \sin^2\vartheta} + 1 + \cos\vartheta \quad (5)$$

The most important difference between the systems with and without frame is not just the modification $\sin^2\vartheta \to \theta + \sin^2\vartheta$ but the change in configuration space from the sphere S^2 to the torus T^2: the angle ϑ is no longer restricted to the range $[0, \pi]$ but varies along a full circle $[0, 2\pi]$. From the point of view of the mass m alone, this amounts to a twofold covering of its configurations, as (φ, ϑ) and $(\varphi + \pi, 2\pi - \vartheta)$ give the same positions of m. Nevertheless, these two configurations can be distinguished by the position of the frame F and the two-valued variable

$$s = \mathrm{sgn}(\pi - \vartheta) = \begin{cases} +1 & \text{if } 0 < \vartheta < \pi \\ -1 & \text{if } \pi < \vartheta < 2\pi \end{cases} \quad (6)$$

may be introduced to account for this distinction. We call it the system's *spin*. Our physical intuition tells us the pure spherical pendulum should emerge in the limit $\theta \to 0$, but it is by no means obvious how T^2 might suddenly turn into S^2. In fact, we shall see that what happens in this limit is a dynamical decomposition of the torus T^2 into *two* spheres S^2 of opposite spin which share their two poles. While the dynamics allows for transitions between the two spin states in the presence of a massive frame, the spin becomes a conserved quantity in the limit of vanishing θ.

To be a little more precise, the covering of $Q = S^2$ by the configuration space with frame, $Q^F = T^2$, is twofold only outside the poles. The points $\vartheta = 0$ or π are blown up into φ-circles. This is admittedly more than a strict double covering, but the deviation occurs on a subset of measure zero and does not severely change our argument. But note that minimum $V = 0$ and maximum $V = 2$ of the potential no longer occur at points in configuration space but on circles.

The present paper deals mainly with the systems (3) and (5), and with their relationship. The analysis is greatly facilitated by the fact that φ is a cyclic variable in both cases, so L_φ and H are independent constants of motion, and the systems are integrable. This remains true if instead of the mass point m we allow for a rigid body of mass M such that the ϑ-axis is a first principal axis, and the center of mass lies on the 3-axis, a distance c from the fixed point. With θ_1, θ_2, and θ_3 its moments of inertia, the energies T and V are

$$T = {}^1/_2\theta_1\,\dot{\vartheta}^2 + {}^1/_2(\theta^F + \theta_3 + (\theta_2 - \theta_3)\sin^2\vartheta)\dot{\varphi}^2$$

$$V = Mgc(1 + \cos\vartheta) \qquad (7)$$

Scaling energies by Mgc, times by $\sqrt{\theta_1/Mgc}$, and using $\theta := (\theta^F + \theta_3)/\theta_1$, $\theta' := (\theta_2 - \theta_3)/\theta_1$, the dimensionless Lagrangian becomes

$$L = {}^1/_2\dot{\vartheta}^2 + {}^1/_2(\theta + \theta'\sin^2\vartheta)\dot{\varphi}^2 - 1 - \cos\vartheta \qquad (8)$$

In this system, the angular momentum $L_\varphi = (\theta + \theta'\sin^2\vartheta)\dot{\varphi}$ is still a conserved quantity, and the analysis is similar to that of (4). The moments of inertia θ^F and θ_3 act together in lowering the centrifugal potential near $\vartheta = 0$ and π, and to open the way for transitions in spin. The pure spherical pendulum (2) can only be recovered in the limit $\theta^F + \theta_3 \to 0$.

Quite a different type of dynamics is obtained if the φ-axis of the frame F is tilted with respect to the z-axis of the gravitational force, by an angle δ ($0 \le \delta \le \pi/2$). The polar axis of the spherical coordinate system still being the φ-axis, the kinetic energy expressions remain unchanged, but the (scaled) potential now involves both angles ϑ and φ,

$$V = 1 + \cos\vartheta\cos\delta - \cos\varphi\sin\vartheta\sin\delta \qquad (9)$$

The minimum $V = 0$ is not assumed on a circle as before but at the two isolated points $(\varphi, \vartheta) = (0, \pi - \delta)$ and $(\pi, \pi + \delta)$. For $\delta \neq 0$, L_φ is no longer a constant, and the system no longer integrable, as demonstrated in Figure 7.

A common feature of all these systems is the set of three discrete symmetry operations that leave the Lagrangian invariant. The first is time reversal **T**,

$$\mathbf{T}: \quad (\varphi, \vartheta, L_\varphi, L_\vartheta) \to (\varphi, \vartheta, -L_\varphi, -L_\vartheta) \qquad (10)$$

The second general symmetry is invariance under reflection **R** with respect to the vertical plane,

$$\mathbf{R}: \quad (\varphi, \vartheta, L_\varphi, L_\vartheta) \to (-\varphi, \vartheta, -L_\varphi, L_\vartheta) \qquad (11)$$

The third symmetry operation **P** transforms the two spin states into each other,

$$\mathbf{P}: \quad (\varphi, \vartheta, L_\varphi, L_\vartheta) \to (\varphi + \pi, 2\pi - \vartheta, L_\varphi, -L_\vartheta) \qquad (12)$$

The combined discrete symmetry group of the system is the direct Abelian product $\{\mathbf{1}, \mathbf{T}\} \times \{\mathbf{1}, \mathbf{R}\} \times \{\mathbf{1}, \mathbf{P}\}$, of order 8. In the special case where the frame is aligned with gravity, $\delta = 0$, the value of φ does not matter, and **P** may simply be replaced by reflection Π of the angle ϑ,

$$\mathbf{\Pi}: \quad (\varphi, \vartheta, L_\varphi, L_\vartheta) \to (\varphi, 2\pi - \vartheta, L_\varphi, -L_\vartheta) \qquad (13)$$

3. Phase Space Analysis

Consider first the Hamiltonian (3) of the ideal spherical pendulum, with configuration space $Q = S^2$. Its phase space T*Q is foliated by energy surfaces E_h, defined by constant values $h > 0$ of the energy H. The energy surfaces in turn are foliated by invariant 2-tori $\mathcal{T}_{h,l_\varphi}$, where l_φ are the constant values of angular momentum L_φ.

The energy surfaces E_h come in two different topologies, depending on the value of h. For $0 < h < 2$, the accessible region of Q is a disk D^2; hence E_h is a 3-sphere S^3. At high energies $h > 2$, all points of Q can be reached with positive kinetic energy, and hence E_h has the topology of $RP^3 \simeq SO(3)$.[15] At the intermediate value $h = 2$, the energy surface is nonsmooth, containing the equilibrium point of the pendulum in upright standing position.

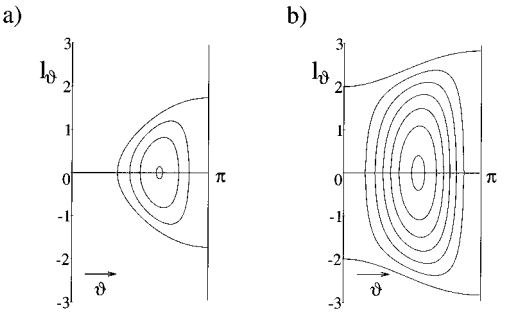

Figure 2. Invariant tori of the spherical pendulum in (ϑ,L_ϑ)-projection, or as Poincaré sections φ = const. The tori are shown at equidistant intervals Δl^2 of $l_\varphi{}^2$, starting with $l_\varphi = 0$ for the outermost torus. (a) $h = 1.5$, typical for low energies where $E_h \simeq S^3$; $\Delta l^2 = 0.5$. (b) $h = 4$, typical for high energies where $E_h \simeq RP^3$; $\Delta l^2 = 1$.

The foliation of E_h by invariant tori is given by the energy equation (3) which for each constant $L_\varphi = l_\varphi$ describes a topological circle in the (ϑ,L_ϑ)-plane; the $\mathcal{T}_{h,l_\varphi}$ are the direct product of these circles with the φ-circles. Figure 2 shows the arrangement of the (ϑ,L_ϑ)-circles for energies $h = 1.5$ and $h = 4$. It may be viewed as a projection of the tori $\mathcal{T}_{h,l_\varphi}$ onto the (ϑ,L_ϑ)-plane; of course, the two signs $L_\varphi = \pm|l_\varphi|$ give the same projections. Alternatively, Figure 2 may be interpreted in terms of Poincaré sections $\varphi = \varphi_0$ where the conditions $\dot{\varphi} > 0$ or < 0 give identical pictures.

The tori $\mathcal{T}_{h,0}$ correspond to planar motion. They are foliated by invariant circles on which φ assumes two constant values, differing by π. (It is an artifact of the singularities of the spherical coordinates that when the motion traverses the poles, the phase space coordinates φ and L_ϑ undergo discontinuous changes to $\varphi + \pi$ and $-L_\vartheta$, respectively.) At energies $h < 2$, these circles are of oscillatory type and may be parametrized with φ from the interval $[0,\pi)$. At energies $h > 2$, the circles are rotations coming in pairs of two directions, related by time reversal. A convenient way to express this situation is to say the torus $\mathcal{T}_{h,0}$ splits in two at the bifurcation $h = 2$. In Figure 2 these tori are represented by the outermost lines. In the Poincaré section interpretation, only one half of the circle $\varphi = \varphi_0 \bmod \pi$ is seen as it lies in the surface of section. The other half of that circle, as well as all other circles of $\mathcal{T}_{h,0}$, is outside the surface of section.

Except for the different topological structure of the two energy surfaces and the splitting of the $l_\varphi = 0$ torus, the pictures of Figure 2, a and b, are very similar. All tori with $l_\varphi \neq 0$ are combinations of φ-rotations with ϑ-oscillations. The amplitude of the latter vanishes at the maximum value $l_{\varphi 0}{}^2$ of $l_\varphi{}^2$ at given h which is obtained by looking for the critical point $(\vartheta, L_\vartheta) = (\vartheta_0, 0)$ of the Hamiltonian (3), at fixed l_φ:

$$\cos\vartheta_0 = {}^1/_3(h - 1) - {}^1/_3\sqrt{(h-1)^2 + 3}$$

$$l_{\varphi 0}{}^2 = 2\sin^2\vartheta_0(h - 1 - \cos\vartheta_0) \qquad (14)$$

In the low- and high-energy limits, these conditions for pure φ-rotation reduce to

$$\cos\vartheta_0 \approx -1 + h/2, \quad l_{\varphi 0}{}^2 \approx h^2 \qquad \text{if } h \to 0$$

$$\cos\vartheta_0 \approx -\frac{1}{2(h-1)}, \quad l_{\varphi 0}{}^2 \approx 2(h-1) \qquad \text{if } h \to \infty \qquad (15)$$

Let us now turn to the Hamiltonian (5) whose configuration space is T^2. The bifurcation scheme of its energy surfaces E_h

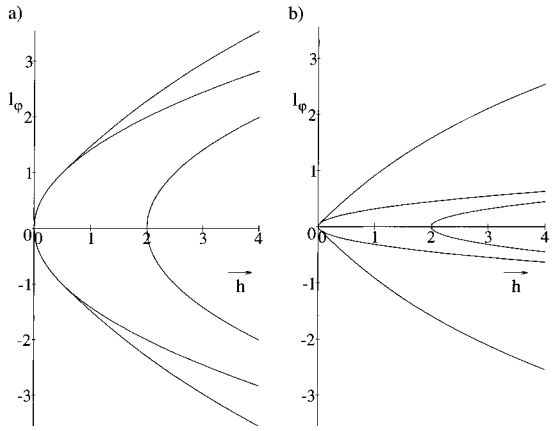

Figure 3. Bifurcation diagram in the (h,l_φ)-plane of constants of motion: (a) $\theta = 1$, (b) $\theta = 0.05$.

and invariant tori $\mathcal{T}_{h,l_\varphi}$ is more interesting than that of the spherical pendulum without frame. At energies $h < 2$, the accessible part of Q is an annulus; hence $E_h \simeq S^2 \times S^1$. At $h > 2$ where all of Q can be reached, $E_h \simeq T^2 \times S^1 = T^3$. The same conclusion may be drawn from the energy equation (5) in the form

$$L_\vartheta^{\,2} = \frac{2(1+\theta-\cos^2\vartheta)(h-1-\cos\vartheta) - l_\varphi^{\,2}}{1+\theta-\cos^2\vartheta} \quad (16)$$

it describes a surface in $(\vartheta,L_\vartheta,L_\varphi)$-space which is topologically a sphere S^2 or a torus T^2, depending on whether h is smaller or larger than 2. Taking the direct product with the φ-circle S^1, we confirm the above assertion about the topology of the energy surface.

The projection of E_h onto the (ϑ,L_ϑ)-cylinder is a disk D^2 for $h < 2$, and an annulus $D^1 \times S^1$ for $h > 2$. Its boundary ($l_\varphi = 0$)

$$L_\vartheta = \sqrt{2(h - 2\cos^2(\vartheta/2))} \quad (17)$$

bifurcates from one to two circles at $h = 2$ where it equals $\pm 2\sin(\vartheta/2)$. At energy $h = 2$ there exists a φ-circle of equilibrium points.

The invariant tori $\mathcal{T}_{h,l_\varphi}$ are direct products of the φ-circle S^1 and the circles given by eq 16 with fixed (h, l_φ). Their bifurcations are obtained from the relative equilibria, i.e., the stationary points of the ϑ-motion. They come in three kinds of isolated periodic orbits:

(i) as φ-rotation in the hanging position $\vartheta = \pi$, $\cos\vartheta = -1$:

$$l_\varphi^{\,2} = l_{s1}^{\,2} := 2\theta h, \quad h \geq 0 \quad (18)$$

(ii) as φ-rotation in the upright position $\vartheta = 0$, $\cos\vartheta = 1$:

$$l_\varphi^{\,2} = l_{s2}^{\,2} := 2\theta(h-2), \quad h \geq 2 \quad (19)$$

(iii) as φ-rotation at a fixed angle ϑ_m where L_ϑ^2 as a function of $\cos\vartheta$ has a relative maximum,

$$\cos\vartheta_m = {}^1\!/_3(h-1) - {}^1\!/_3\sqrt{(h-1)^2 + 3(1+\theta)} \quad (20)$$

$$l_\varphi^{\,2} = l_m^{\,2} := 2(1+\theta-\cos^2\vartheta_m)(h-1-\cos\vartheta_m), \quad h \geq \theta/2 \quad (21)$$

Combining these results, we obtain the bifurcation diagram of Figure 3. Three different energy ranges must be distinguished, depending on the manner in which E_h is foliated by invariant tori. At low energies $0 < h < \theta/2$, there is only one family of tori $\mathcal{T}_{h,l_\varphi}$, the angular momentum l_φ ranging from $-l_{s1}$ to $+l_{s1}$. Figure 4a shows their projection onto the (ϑ,L_ϑ)-plane, or equivalently, Poincaré sections $\varphi = \varphi_0$, $\dot\varphi > 0$ (or <0 which gives different tori but identical pictures). The motion is a combination of φ-rotation and ϑ-oscillation about the stable equilibrium position $\vartheta = \pi$. The angular momentum L_φ assumes values from $l_\varphi = 0$, corresponding to pure ϑ-oscillation (outermost circle in Figure 4a), to $l_\varphi = \pm l_{s1}$, corresponding to pure φ-rotation in the hanging position $\vartheta = \pi$. This type of motion does not exist in the isolated spherical pendulum where the centrifugal potential prevents a transition through the poles with finite angular momentum l_φ.

At $h = \theta/2$, there is a pitchfork bifurcation of the rotating periodic orbit in hanging position which becomes unstable and gives birth to two new stable periodic orbits with $\vartheta = \text{const} \neq 0$. Consequently, in the energy range $\theta/2 < h < 2$, there are two kinds of tori $\mathcal{T}_{h,l_\varphi}$; see Figure 4b. For $0 < l_\varphi^{\,2} < l_{s1}^{\,2}$, the tori are a continuation of the low-energy type; the corresponding motion is ϑ-oscillation through the south pole, plus φ-rotation. At $l_\varphi^{\,2} = l_{s1}^{\,2}$ there is a separatrix, and for larger $l_\varphi^{\,2}$, two tori exist for each l_φ, one with $\vartheta < \pi$, the other with $\vartheta > \pi$. These tori are mirror images of each other under the spin transformation **P**. Apart from the π-shift in the frame position φ, they describe the same physical situation. The motion of the mass point m is qualitatively identical to that of the pure spherical pendulum, namely, ϑ-oscillation avoiding the poles, combined with φ-rotation.

The high-energy range $h > 2$ exhibits yet another type of torus at low values of l_φ; see Figure 4c. The new pairs of tori appear in connection with the topological bifurcation of the energy surface. For $l_\varphi^{\,2} < l_{s2}^{\,2}$, there is rotational ϑ-motion passing through the north pole $\vartheta = 0$. At given l_φ, the members of a pair are related by the symmetry **RT**. In the ideal spherical

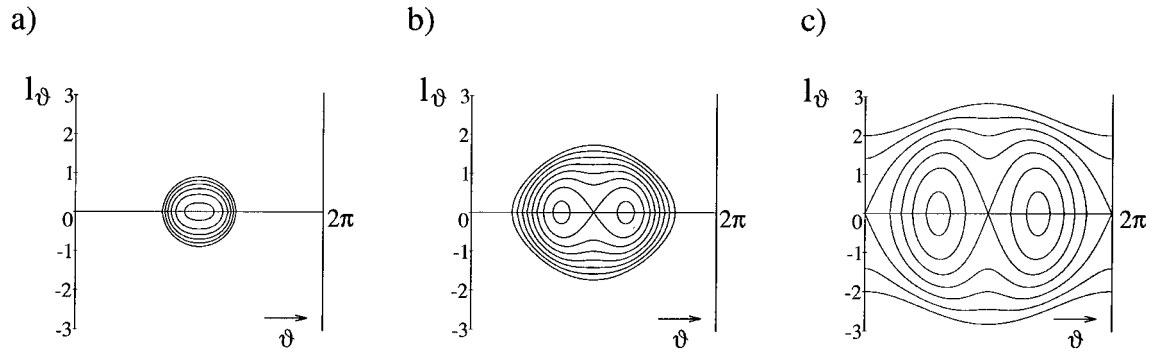

Figure 4. Projection of invariant tori $\mathcal{T}_{h,l_\varphi}$ onto the (ϑ,L_ϑ)-plane, for three different energies h. The moment of inertia of the frame is $\theta = 1$. (a) $h = 0.4$, $\Delta l^2 = 0.15$; (b) $h = 1.5$, $\Delta l^2 = 0.5$; (c) $h = 4$, $\Delta l^2 = 2$.

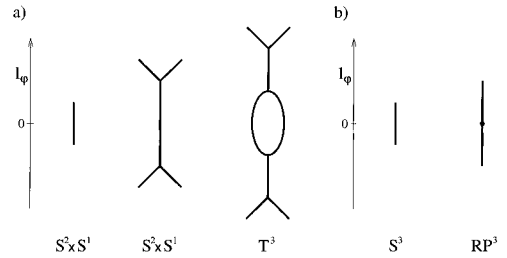

Figure 5. Fomenko graphs of the different types of energy surfaces for $\theta < 4$: (a) spherical pendulum with frame; energy ranges are $0 < h < \theta/2$ (left), $\theta/2 < h < 2$ (middle), and $h > 2$ (right); (b) pure spherical pendulum at energies $h < 2$ (left) and $h > 2$ (right). The vertical axis is l_φ. Each torus $\mathcal{T}_{h,l_\varphi}$ is represented by a point on the corresponding graph. Bifurcations of tori appear as vertices.

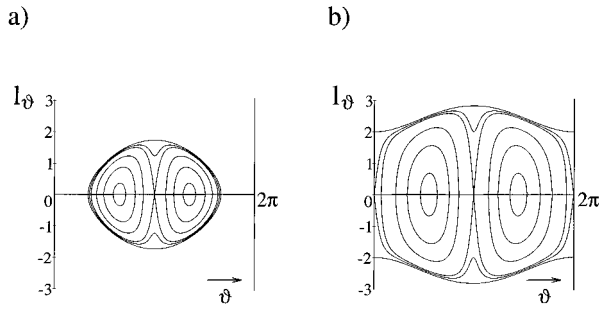

Figure 6. (ϑ,L_ϑ)-projection of invariant tori $\mathcal{T}_{h,l_\varphi}$ for $\theta = 0.05$: (a) $h = 1.5$, $\Delta l^2 = 0.5$; the torus ${l_\varphi}^2 = 0.075$ and the separatrix ${l_\varphi}^2 = {l_{s1}}^2 = 0.15$ are also shown; (b) $h = 4$, $\Delta l^2 = 2$; the two separatrices ${l_\varphi}^2 = {l_{s1}}^2 = 0.4$ and ${l_\varphi}^2 = {l_{s2}}^2 = 0.2$ are also shown.

pendulum, there is only one torus of this kind, for $l_\varphi = 0$, because otherwise the centrifugal barrier prevents access to the poles.

A schematic view of the ordering of tori in phase space may be given in terms of Fomenko graphs[16,17] as shown in Figure 5. Each graph represents an energy surface $H = h$, and depending on the value of h, there are three types. Points of the diagram are in (1:1) correspondence with tori $\mathcal{T}_{h,l_\varphi}$. The vertical axis is the angular momentum l_φ, with ranges $[-l_{s1}, l_{s1}]$ at energies $h < \theta/2$, and $[-l_m, l_m]$ at larger energies. The bifurcations at ${l_\varphi}^2 = {l_{s1}}^2$ (for $h > \theta/2$) and ${l_\varphi}^2 = {l_{s2}}^2$ (for $h > 2$) appear as vertices. Time reversal symmetry **T** is expressed as mirror symmetry with respect to the horizontal axis $l_\varphi = 0$. The outer legs are related by spin symmetry **P**, the two branches of the inner loop by reflection symmetry **RT**.

Fomenko graphs for the frameless spherical pendulum are shown in Figure 5b. Their $l_\varphi > 0$ and $l_\varphi < 0$ halves each correspond to one leg—one spin state—of the outer parts of Figure 5a. At $l_\varphi = 0$, the dot in the high-energy graph of Figure 5b is a leftover from the loop in Figure 5a, symbolizing the transition from ϑ-oscillation to rotation.

Let us now ask how the two systems (3) and (5) are related in the limit $\theta \to 0$ of vanishing moment of inertia of the Cardan frame. Comparison of Figure 3, a and b, gives an indication. As $\theta \to 0$, the low-energy part $h < \theta/2$ becomes vanishingly small, and the separatrices ${l_\varphi}^2 = {l_{s1,2}}^2$ are squeezed against the axis $l_\varphi = 0$. In the limit $\theta = 0$ the bifurcation diagram reduces to the lines (14) plus the singular line $l_\varphi = 0$. Figure 6 shows how the system of tori behaves at small θ. Motion that penetrates the centrifugal barriers at the poles $\vartheta = 0$ and/or π covers a negligible part of phase space. The tori with ${l_\varphi}^2 > {l_{s1}}^2$ become more and more similar to those of the ideal spherical pendulum, except that they appear in two spin states.

In order to quantify these statements, and to develop a picture for the effective reduction of configuration space by a factor of 2, we need to determine the actions (I_φ, I_ϑ) of the tori $\mathcal{T}_{h,l_\varphi}$. This is the subject of the next section.

Let us take a brief look on what happens when the supporting frame is tilted by an angle δ with respect to the vertical axis. The potential (9) now depending on both angles ϑ and φ, the angular momentum L_φ is no longer conserved; hence one expects the system to be nonintegrable. This is corroborated by the Poincaré sections shown in Figure 7. Compared to Figure 6b ($\delta = 0$), we observe the following changes.

(i) The separatrices dissolve into chaotic bands, the chaos getting more pronounced as δ increases.

(ii) The Π-symmetry with respect to ϑ-reflection at constant φ is lost; however, the system is still invariant under the transformation **P**, cf. ref 12.

(iii) The two orbits (of opposite spin) with maximum ${l_\varphi}^2$ at $\delta = 0$ lose their stability to two other orbits (again of opposite spin) which in the fully tilted position $\delta = \pi/2$ are planar pendulum rotations of the angle φ, at fixed $\vartheta = \pi/2$ or $3\pi/2$. Nothing of this rich dynamical behavior is seen if the frame is absent from the start, $\theta = 0$. It would only appear inappropriate to choose the polar axis of spherical coordinates tilted against the direction of gravity. Yet even the smallest nonzero θ makes different angles δ physically inequivalent. There is no space here to explore the interesting dependence of the dynamics on combinations of the parameters δ, θ, h. Suffice it to say that very little of the following can be applied to the chaotic regions of phase space and that insight into the corresponding quantum mechanics is as of now completely lacking.

4. Action Integrals

As the Hamiltonians (3) and (5) describe integrable systems, canonical transformations $(\varphi, \vartheta, L_\varphi, L_\vartheta) \to (\phi_1, \phi_2, I_1, I_2)$ to action-angle variables may be found such that the new Hamiltonians $H = H(I_1, I_2)$ depend only on the actions I_k, and the dynamics becomes trivial: $I_k = \text{const}$, $\dot{\phi}_k = \omega_k = \partial H/\partial I_k = \text{const}$. Because of the trivial separability into φ- and ϑ-motion, the action integrals $I_1 = I_\varphi$ and $I_2 = I_\vartheta$ are easily identified as contour integrals along the two fundamental paths of the invariant tori $\mathcal{T}_{h,l_\varphi}$,

$$I_\varphi = \frac{1}{2\pi}\oint \gamma_\varphi L_\varphi \, \mathrm{d}\varphi = l_\varphi \tag{22}$$

$$I_\vartheta = \frac{1}{2\pi}\oint \gamma_\vartheta L_\vartheta \, \mathrm{d}\vartheta \tag{23}$$

To evaluate the last integral, we must insert eq 16, with $\theta = 0$ for the ideal spherical pendulum.

The frequency $\omega_2 = \omega_\vartheta = 2\pi/T_\vartheta$ is obtained from

$$T_\vartheta = \oint \gamma_\vartheta \frac{\partial L_\vartheta}{\partial h}\Big|_{l_\varphi} \mathrm{d}\vartheta \tag{24}$$

and the frequency of φ-motion is best calculated from the winding ratio

$$W := \frac{\omega_\varphi}{\omega_\vartheta} = \frac{\partial H/\partial I_\varphi}{\partial H/\partial I_\vartheta} = -\frac{\partial I_\vartheta}{\partial I_\varphi}\Big|_h \tag{25}$$

Let us go through these calculations step by step. Inserting eq 16 and using $z = \cos\vartheta$, we get

$$I_\vartheta = \frac{n}{2\pi}\int_{z_1}^{z_2} \sqrt{\frac{2f(z)}{g(z)}}\,\mathrm{d}z \tag{26}$$

where the limits of integration z_1 and z_2 and the numbers n of

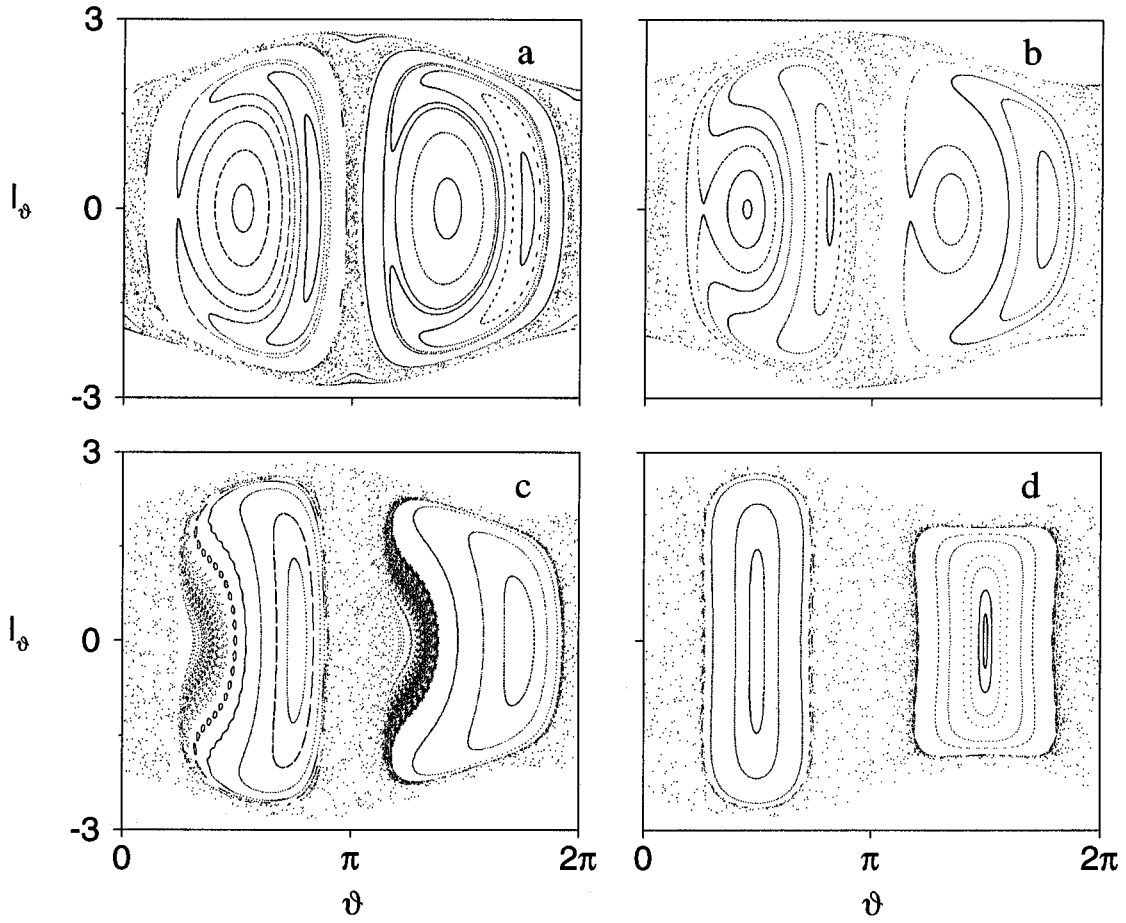

Figure 7. Poincaré sections $\varphi = 0$, $\dot{\varphi} > 0$, for $h = 4$ and small angular momentum of the frame, $\theta = 0.05$, with tilt angle (a) $\delta = 0.1$, (b) $\delta = 0.3$, (c) $\delta = 0.6$, (d) $\delta = \pi/2$.

pieces in a closed path will be determined later. The functions $f(z)$ and $g(z)$ are the polynomials

$$f(z) = (1 + \theta - z^2)(h - 1 - z) - {}^1/_2 l_\varphi{}^2 \qquad (27)$$

$$g(z) = (1 + \theta - z^2)(1 - z^2)$$

The period T_ϑ is the integral

$$T_\vartheta = n \int_{z_1}^{z_2} \sqrt{\frac{g(z)}{2f(z)}} \frac{\mathrm{d}z}{1 - z^2} \qquad (28)$$

and the winding ratio

$$W = \frac{n}{2\pi} l_\varphi \int_{z_1}^{z_2} \sqrt{\frac{1}{2f(z)g(z)}}\, \mathrm{d}z \qquad (29)$$

In the general case $\theta \neq 0$ the integrands have seven branch points which makes the integrals hyperelliptic. There is no hope for analytic integration, and we must turn to numerical evaluation. In the limit $\theta = 0$, however, the four branch points provided by $g(z)$ disappear, as $[g(z)]^{1/2} \rightarrow 1 - z^2$, and the integrals are elliptic. The simplest of these integrals is T_ϑ:

$$T_\vartheta = 2 \int_c^b \frac{\mathrm{d}z}{2(a - z)(b - z)(z - b)} = \frac{2\sqrt{2}}{\sqrt{a - c}} K(k) \qquad (30)$$

where $a > b > c$ are the zeroes of $f(z)$ and $K(k)$ is the complete elliptic integral of the first kind, with modulus $k = [(b - c)/(a - c)]^{1/2}$.

The winding ratio (29) of the pure spherical pendulum is obtained after decomposing $1/(1 - z^2)$ into its partial fractions:

$$W = \frac{l_\varphi}{\pi\sqrt{2(a - c)}} \left(\frac{1}{1 - c} \Pi(\alpha_-, k) + \frac{1}{1 + c} \Pi(\alpha_+, k) \right) \qquad (31)$$

where $\Pi(\alpha, k)$ is the complete elliptic integral of the third kind, the parameters being $\alpha_\pm = (b - c)/(\pm 1 - c)$.

Finally, the action integral (26) is evaluated with the partial fraction decomposition

$$\frac{f(z)}{1 - z^2} = -z + h - 1 - {}^1/_4 l_\varphi{}^2 \left(\frac{1}{1 - z} + \frac{1}{1 + z} \right) \qquad (32)$$

the result is

$$I_\vartheta = \frac{4}{\pi\sqrt{2(a - c)}} ((a - c)E(k) + (h - 1 - a)K(k)) - l_\varphi W \qquad (33)$$

where $E(k)$ is the complete elliptic integral of the second kind.

The limits of low and high energies can be treated by elementary integration. We leave it as an exercise to show that

$$H \approx |I_\varphi| + 2I_\vartheta \qquad \text{for } h \rightarrow 0$$

$$H \approx {}^1/_2 (|I_\varphi| + I_\vartheta)^2 \qquad \text{for } h \rightarrow \infty \qquad (34)$$

For the frequencies ω_φ, ω_ϑ, and their ratio W, this implies

$$\omega_\varphi = \mathrm{sgn}(l_\varphi) \qquad \omega_\vartheta = 2 \qquad W = \pm {}^1/_2 \qquad (35)$$

in the limit of low energies, and

$$\omega_\varphi = \sqrt{2h}\,\mathrm{sgn}(l_\varphi) \qquad \omega_\vartheta = \sqrt{2h} \qquad W = \pm 1 \tag{36}$$

at high energies.

The limit $l_\varphi \to 0$ is familiar from the simple pendulum. We must distinguish the energy ranges $h < 2$ and $h > 2$. At low energies, $a = 1$, $b = h - 1$, $c = -1$, and hence $k = [h/2]^{1/2}$ and

$$T_\vartheta = 2K(k), \quad I_\vartheta = (4/\pi)(E(k) - (1 - k^2)K(k)) \qquad (l_\varphi = 0;\ h < 2) \tag{37}$$

Note that a ϑ-period is defined here to extend from minimum to maximum and back; in an oscillating pendulum the period is usually taken to be twice as large. At high energies, a and b are exchanged, hence $k = [2/h]^{1/2}$, and

$$T_\vartheta = 2k\,K(k), \quad I_\vartheta = (4/\pi k)E(k) \qquad (l_\varphi = 0;\ h > 2) \tag{38}$$

The $l_\varphi \to 0$ limit of the winding ratio (31) is delicate because the integral in eq 29 diverges as the lower limit $z_1 = c \approx l_\varphi{}^2/4h$ tends to zero. Careful analysis shows that $|W| \to 1/2$ for $h < 2$, and $|W| \to 1$ for $h > 2$.

Another limit that may be worked out in detail is that of pure φ-rotation where $l_\varphi{}^2$ assumes its maximum value $l_{\varphi 0}{}^2$ given in eq 14. The zeroes of $f(z)$ are then

$$a = {}^1/_3(h-1) + {}^2/_3\sqrt{(h-1)^2 + 3}, \qquad b = c = {}^1/_3(h-1) - {}^1/_3\sqrt{(h-1)^2 + 3} \tag{39}$$

and modulus k as well as parameters $\alpha_\pm$ are zero. With $K(0) = E(0) = \Pi(0,0) = \pi/2$, we find $I_\vartheta = 0$, and for the frequencies

$$\omega_\vartheta = \sqrt{2(a-c)} = \sqrt{2}((h-1)^2 + 3)^{1/4},$$

$$\omega_\varphi = \sqrt{\frac{2(h-1-c)}{1-c^2}} \tag{40}$$

Figures 8−10 are graphical representations of the above results. The frequencies ω_ϑ and ω_φ are shown as contour plots in the (h,l_φ)-plane in Figure 8. They both vanish at the singular point $(h, l_\varphi) = (2, 0)$ where the asymptotic behavior along the energy axis is $\omega_\vartheta = 2\pi/(5 \ln 2 - \ln|h-2|)$. The oscillatory ϑ-motion has positive frequencies everywhere whereas the rotational φ-motion has positive or negative frequencies, depending on the sign of l_φ.

Figure 9 shows the energy surfaces $H(I_\varphi, I_\vartheta) = h$ as contour lines in the (I_φ, I_ϑ)-plane of action variables. The asymptotic linear behavior $I_\vartheta \approx (h - |I_\varphi|)/2$ at low energies, and $I_\vartheta \approx (2h)^{1/2} - |I_\varphi|$ at high energies as given in eq 34, is well borne out. The singular point $(I_\varphi, I_\vartheta, h) = (0, 4/\pi, 2)$ is much less conspicuous here than in the frequency pictures. But taking the derivative along lines of constant energy h gives it a prominent appearance. This is done in Figure 10 where the winding ratio W is plotted as a function of l_φ, for a number of different energies. (Only the positive l_φ part is shown, as $W(h,-l_\varphi) = -W(h,l_\varphi)$.) The figure is a kind of link between the two other pictures because W is at the same time the ratio $\omega_\varphi/\omega_\vartheta$ and the negative slope of the energy surfaces; see eq 25. The situation is considerably more complicated if the spherical pendulum is suspended in a frame with moment of inertia θ. However, combining the insight provided by Figure 4 with numerical integration of eqs 26, 28, and 29, it is straightforward to obtain a comprehensive picture of the dynamics. Let us start with a discussion of the

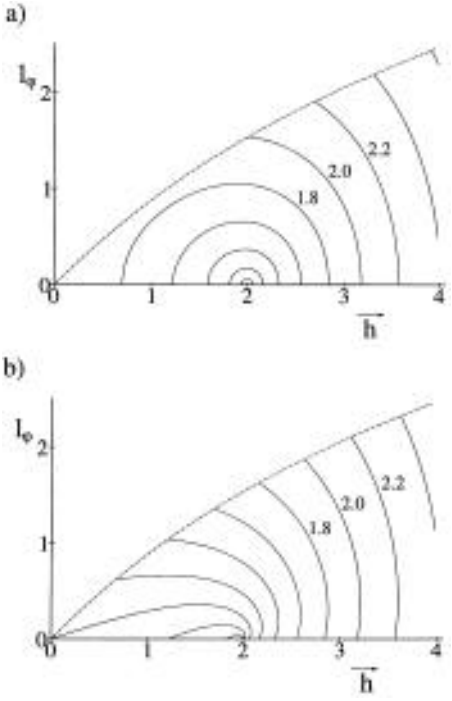

Figure 8. Contour lines of constant frequencies ω_ϑ (a) and ω_φ (b) in the plane (h, l_φ) of constants of motion, for the frameless spherical pendulum, $\theta = 0$.

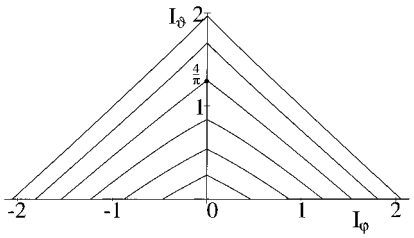

Figure 9. Energy surfaces of the spherical pendulum without frame, in action variable representation $H(I_\varphi, I_\vartheta) = h$. The values of h are multiples of 0.5. Corresponding to the oscillatory nature of the ϑ-motion, I_ϑ is always positive, whereas there are two signs for I_φ depending on the sense of the rotation.

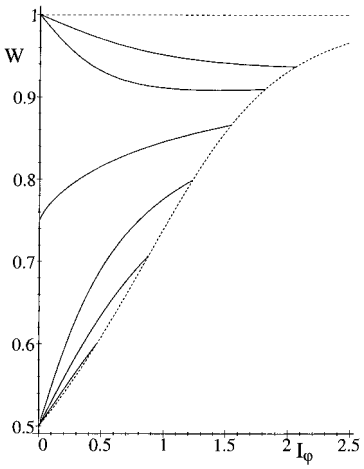

Figure 10. Winding ratios W as functions of I_φ, for the same constant values of energy h as in Figure 9. Only the positive branch of the graph is shown. The values of W range from $^1/_2$ to 1.

action variables, and consider Figure 11 which is the analogue of Figure 9. Remember that the angle ϑ can now vary from 0 to 2π.

At low energies, $h \ll \theta$, the Hamiltonian (5) may be expanded to second order in the phase space variables. The motion is

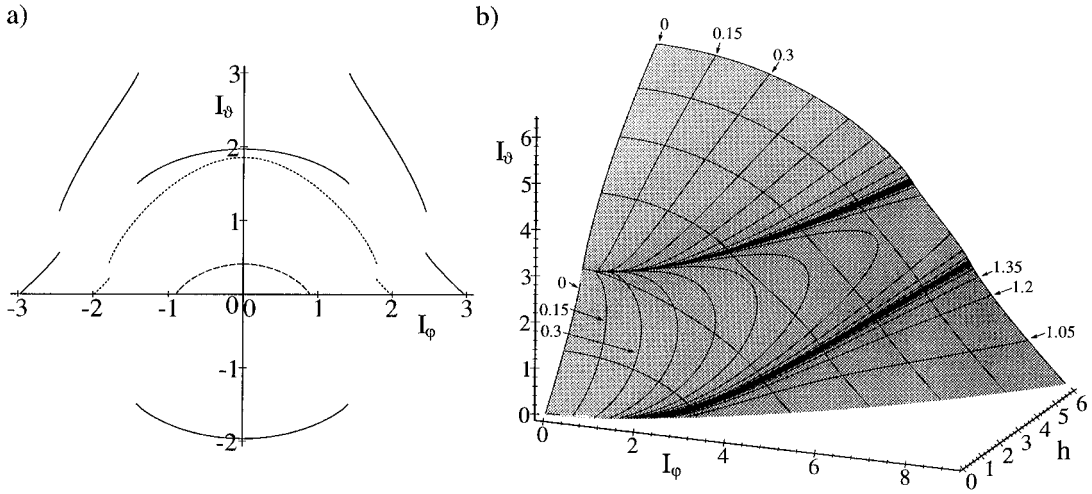

Figure 11. Energy surfaces of the spherical pendulum with frame, $\theta = 1$: (a) 2-D representation in the (I_φ, I_ϑ)-plane for three values of the energy; $h = 0.4$ (one dashed line), $h = 1.6$ (three pieces of dotted line), $h = 3.0$ (six pieces of full line). The action of rotational motion appears with two signs. Only one of the two spin states at the high-$I_\varphi{}^2$ ends is shown. (b) 3-D representation in $(I_\varphi, I_\vartheta, h)$-space. The actions I_ϑ are combined in such a way that the surface is continuous; notice the weak logarithmic slope singularities at the separatrices. The surface carries contour lines of constant h and winding number W. Along $I_\varphi = 0$, the winding number is 0; it increases in steps of 0.15.

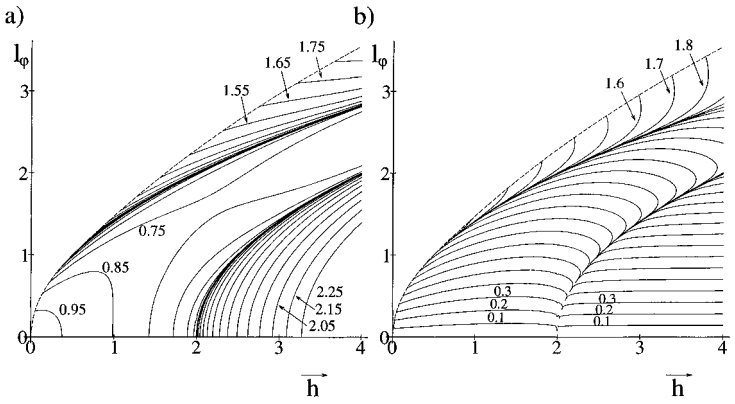

Figure 12. Contour lines in equal steps of constant frequencies ω_ϑ (left) and ω_φ (right) in the plane (h, l_φ) of constants of motion, for $\theta = 1$. The separatrices are well borne out.

then a combination of φ-rotations with ϑ-oscillations about the equilibrium position $\vartheta = \pi$. In action variables, we find

$$H = I_\vartheta + \frac{1}{2\theta} I_\varphi{}^2 \tag{41}$$

This explains the parabolic shape of the energy surfaces at low h.

Between $h = \theta/2$ and $h = 2$, there are two types of motion. The low-l_φ branch, $l_\varphi{}^2 < l_{s1}{}^2 = 2\theta h$, is a continuation of the low-energy motion. As $I_\varphi{}^2 = l_\varphi{}^2$ grows beyond the separatrix value $l_{s1}{}^2$, the invariant tori split into two sets with spherical pendulum type of motion, each with a definite spin state. The ϑ-oscillations are now about ϑ_m as given in eq 20 and do not reach the poles $\vartheta = \pi$ or 0. The action I_ϑ for an individual torus jumps by a factor $^1/_2$, with the sum rule $I^-_{\vartheta,s1} := I_\vartheta(\pm[l_{s1}{}^2-]^{1/2}) = 2I^+_{\vartheta,s1} := 2I_\vartheta(\pm[l_{s1}{}^2+]^{1/2})$, see Figure 11a; in the 3-D representation of Figure 11b we have added the actions of the two spin states so as to make the surface continuous across the separatrix.

Beyond the bifurcation of the energy surface at $h = 2$, and at low angular momenta, $l_\varphi{}^2 < l_{s2}{}^2 = 2(h - 2)\theta$, rotational ϑ-motion appears. The two senses of the rotation correspond to the two signs of I_ϑ in Figure 11a, and the sum rule at the separatrix is $I^+_{\vartheta,s2} := I_\vartheta(\pm[l_{s2}{}^2+]^{1/2}) = 2|I^-_{\vartheta,s2}| := 2|I_\vartheta(\pm[l_{s2}{}^2-]^{1/2})|$. Adding the absolute values of these two branches of the energy surface, we obtain the continuous picture of Figure 11b.

For $l_\varphi = 0$, the motion is that of an ordinary pendulum, and I_ϑ will be denoted by $I_{\vartheta,0}$. Compared to the situation without frame, however, the ϑ-range $\vartheta > \pi$ also contributes to a full period. This adds a factor 2 to the low-energy results in eq 37, $I_{\vartheta,0} = (8/\pi)(E(k) - (1 - k^2)K(k))$, while those of eq 38 must be taken with the two signs, $I_{\vartheta,0} = \pm(4/\pi k)E(k)$.

Figure 12 is the result of numerical computations for the frequencies ω_ϑ and ω_φ using eqs 28 and 29, together with 27 for $\theta = 1$. The pictures should be compared to Figure 8; they are dominated by the nonspherical pendulum types of motion.

Let us now discuss the limit of vanishing moment of inertia θ. Figure 13 for $\theta = 0.05$, if compared to Figure 11b, shows how the low-l_φ types of motion and the two separatrices get squeezed toward the $I_\varphi = 0$ axis. The only tori to survive in the limit $\theta \to 0$, at $l_\varphi \neq 0$, are those with ideal spherical pendulum motion, and definite spin state. Transitions between the two spin states do not occur.

A suggestive picture for the transition from configuration space $Q^F = T^2$ to two spheres $Q = S^2$, of opposite spin state, may be obtained in the following way. Drawing the (φ, ϑ)-torus as a doughnut in R^3, $(\varphi, \vartheta) \to (x, y, z) = ((A + R(\vartheta) \cos \varphi) \cos \vartheta, (A + R(\vartheta) \cos \varphi) \sin \vartheta, R(\vartheta) \sin \varphi)$, we choose a ϑ-dependent radius $R(\vartheta)$ such that the cross section πR^2 of the torus at given ϑ is proportional to the total action of that part of phase space which connects to the given ϑ by Liouville tori. All tori with $0 \leq l_\varphi{}^2 \leq l_{s2}{}^2$ reach the north pole $\vartheta = 0$; hence

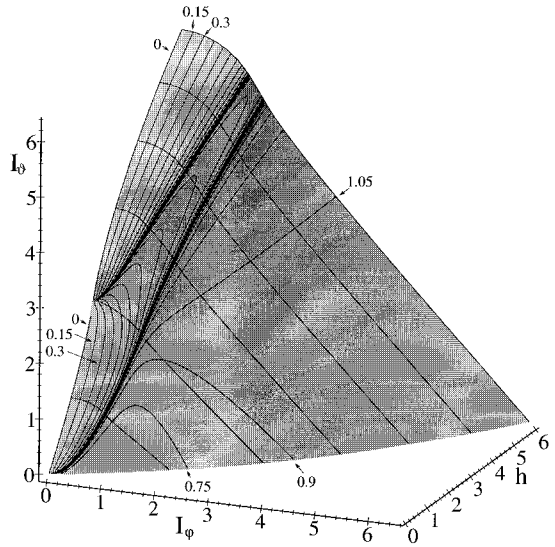

Figure 13. Energy surfaces of the spherical pendulum with frame, $\theta = 0.05$, in 3-D representation as in Figure 11b. The contour lines of constant winding ratio are shown in steps of 0.15.

$R^2(0) = 2(|I_{\vartheta,0}| - |I^-_{\vartheta,s2}|)$. For angles $0 < \vartheta < \pi$ let us define $I_\vartheta(\vartheta)$ as the action I_ϑ of the torus $\mathcal{T}_{h,l_\varphi}$ which has $L_\vartheta = 0$ at the given ϑ: from eq 16 this implies $l_\varphi^2 =: l_\varphi^2(\vartheta) = 2(1 + \theta - \cos^2\vartheta)(h - 1 - \cos\vartheta)$. The separatrix $l_\varphi^2 = l_{s1}^2$ spans angles ϑ in the range $\cos\vartheta \le \cos\vartheta_{s1} = (h - [(h-2)^2 + 4\theta]^{1/2})/2$; hence at angles $0 \le \vartheta \le \vartheta_{s1}$ we see all tori with $l_\varphi^2 < l_\varphi^2(\vartheta)$, and $R^2(\vartheta) = 2|I_{\vartheta,0}| - I_\vartheta(\vartheta)$. For larger angles, $\vartheta_{s1} < \vartheta < \pi$, only one spin state is seen, and $R^2(\vartheta) = 2|I_{\vartheta,0}| - I^+_{\vartheta,s1} - I_\vartheta(\vartheta)$. This goes through a maximum at $\vartheta = \vartheta_m$ (see eq 20) and ends in the value $R^2(\pi) = 2(|I_{\vartheta,0}| - |I^+_{\vartheta,s1}|)$. In the range $\vartheta > \pi$ we have $R(\vartheta) = R(2\pi - \vartheta)$.

Figure 14 shows the tori so constructed for $\theta = 0.05$ and $\theta = 0.0001$. The "dynamic weight" of the poles obviously shrinks as the frame becomes lighter and lighter, and in the limit $\theta \to 0$ the configuration space effectively splits into two topological spheres held together at the two poles.

5. Quantum Spectra

The Schrödinger equation for the spherical pendulum, including the frame, is obtained from eq 5 with $L_\vartheta \to -i\hbar\partial/\partial\vartheta$ and $L_\varphi \to -i\hbar\partial/\partial\varphi$, where $\hbar$ is measured in units of $mr\sqrt{gr}$. The standard separation ansatz for the wave function, $\Psi(\varphi, \vartheta) = \psi(\vartheta)e^{im\varphi}$, $m = 0,\pm1,\pm2,...$, leads to the one-dimensional eigenvalue problem

$$\left(-\frac{\hbar^2}{2}\frac{\partial^2}{\partial\vartheta^2} + V(\vartheta)\right)\psi(\vartheta) = E\psi(\vartheta) \tag{42}$$

with effective potential

$$V(\vartheta) = 1 + \cos\vartheta + \frac{\hbar^2}{2}\frac{m^2}{\theta + \sin^2\vartheta} \tag{43}$$

and boundary conditions $\psi(\vartheta) = \psi(\vartheta + 2\pi)$ and $\psi'(\vartheta)$ continuous. $V(\vartheta)$ on the circle $0 \le \vartheta \le 2\pi$ has reflection symmetry $\hat{\mathbf{\Pi}}$, hence the eigenfunctions can be chosen to have even or odd parity $\Pi = \pm1$,

$$\hat{\mathbf{\Pi}}\psi^\pm = \Pi\psi^\pm: \quad \psi^+(\vartheta) = \psi^+(-\vartheta), \quad \psi^-(\vartheta) = -\psi^-(-\vartheta) \tag{44}$$

As there is no analytic solution to eq 42, one possibility to obtain spectra and eigenfunctions is to use a shooting method for brute force numerical computation. Alternatively, semiclassical procedures have been available for some time which are almost as good. We have performed both types of calculation to obtain the spectra shown here and on the scale of resolution of these pictures found no differences.

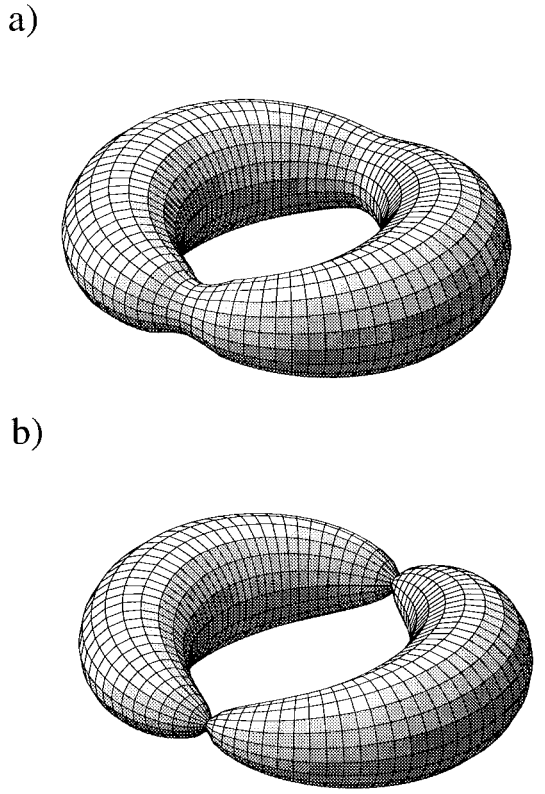

Figure 14. (φ,ϑ)-configuration space of the spherical pendulum with frame, for two values of the moment of inertia θ: (a) $\theta = 0.05$, (b) $\theta = 0.0001$. The cross section $\pi R^2(\vartheta)$ of the configuration space torus at given ϑ is a measure of the phase space weight of the Liouville tori that reach this value of ϑ.

The presence of separatrices typically leads to discontinuities in the standard semiclassical quantization schemes. This is avoided in a method worked out by Miller[18,19] to obtain a uniform quantization condition. It combines the WKB method with an elegant procedure to connect pieces of the solution at deflection points ϑ (real or complex), where the energy equals the value of the effective potential. As this method is particularly well suited for our kind of problem we briefly recall its main ingredients. Let V_m be the minimum value of the potential, $V_m = V(\vartheta_m) = V(2\pi - \vartheta_m)$, and $V_1 = V(\pi)$, $V_2 = V(0)$ its two maxima, $V_2 = V_1 + 2$. For energies E in the range (V_m, V_1), there are four classical turning points, i.e., real solutions ϑ_i to the equation $V(\vartheta) = E$. Let their arrangement be $0 < \vartheta_1 < \vartheta_m < \vartheta_2 < \pi$ and $\vartheta_3 = 2\pi - \vartheta_2$, $\vartheta_4 = 2\pi - \vartheta_1$. Three integrals must be computed, the classical action integral I_ϑ, and two tunnel integrals T_1, T_2:

$$I_\vartheta = \frac{2}{\pi}\int_{\vartheta_1}^{\vartheta_2} L_\vartheta\,\mathrm{d}\vartheta, \quad T_1 = \int_{\vartheta_2}^{\vartheta_3}\sqrt{-L_\vartheta^2}\,\mathrm{d}\vartheta, \quad T_2 = \int_{\vartheta_4}^{\vartheta_1}\sqrt{-L_\vartheta^2}\,\mathrm{d}\vartheta \tag{45}$$

The quantization condition is then

$$\cos\frac{\pi I_\vartheta}{\hbar} = \frac{e^{-(T_1+T_2)/\hbar} - 1}{\sqrt{(1 + e^{-2T_1/\hbar})\,(1 + e^{-2T_2/\hbar})}} \tag{46}$$

and must be evaluated numerically. For $T_1 \gg \hbar$ and $T_2 \gg \hbar$,

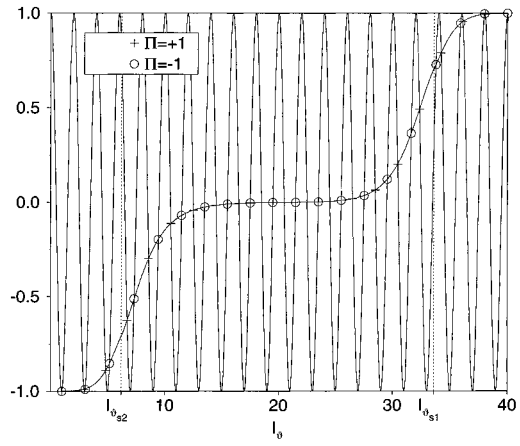

Figure 15. Graphical evaluation of eq 46 for $m = 20$ and $\hbar = 0.1$.

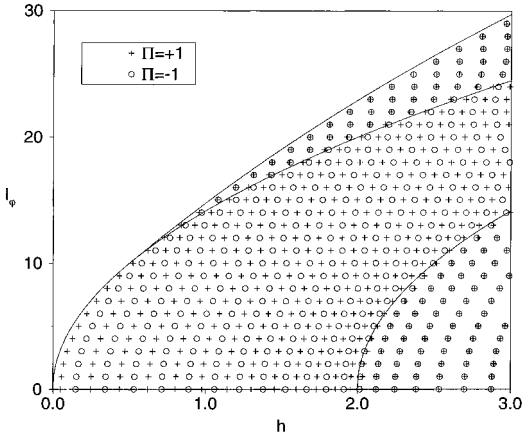

Figure 16. Spectrum of eigenstates of the Schrödinger equation (42) for $\theta = 1$ and $\hbar = 0.1$. The values of $l_\varphi = I_\varphi$ are multiples of $\hbar$; only positive I_φ are shown as the spectrum is symmetric under $I_\varphi \rightarrow -I_\varphi$. The energy eigenvalues were determined by numerical solution and by uniform semiclassical quantization. Crosses are for even, circles for odd eigenfunctions $\psi(\vartheta)$.

the right-hand side (rhs) goes to -1, and we obtain the Bohr−Sommerfeld condition $I_\vartheta = (2n + 1)\hbar$, with twofold degeneracy for each state.

When E is in the range $V_1 < E < V_2$, the angles ϑ_2 and ϑ_3 are complex, and the integral for T_1 must be taken along the imaginary direction. This gives a negative value for T_1, and if both $|T_i|$ are large compared to $\hbar$, the rhs goes to 0. The quantum condition is then $I_\vartheta = (n + {}^1/_2)\hbar$, and there is no degeneracy. For $E > V_2$, the integral T_2 is also negative, and well above the second separatrix the rhs approaches 1. This implies $I_\vartheta = 2n\hbar$, with twofold degeneracy.

Figure 15 shows a typical example where the rhs of eq 46 was first computed as a function of energy E and then transformed to a function of I_ϑ with the help of eq 26. The width of the transition regions around the two separatrices depends on where the tunnel integrals are on the order of $\hbar$.

The spectra for $\theta = 0.05$ and $\theta = 1$ (with $\hbar = 0.1$) are shown in Figures 16 and 17, respectively. Even states are represented as crosses and odd states as circles. Negative values of $I_\varphi = l_\varphi = m\hbar$ are omitted as $V(\vartheta)$ depends on m^2. The three "phases" of the bifurcation diagrams Figure 3 are readily identified. Except near the separatrices which appear somewhat blurred, they are clearly distinguished by the degeneration scheme of even and odd states.

In the low-l_φ phase ${l_\varphi}^2 < {l_{s2}}^2 = 2\theta(h - 2)$, $h > 2$, even and odd states are (nearly) degenerate. This is easy to understand in the limit $l_\varphi = 0$, $h \gg 2$ where the two degenerate states are

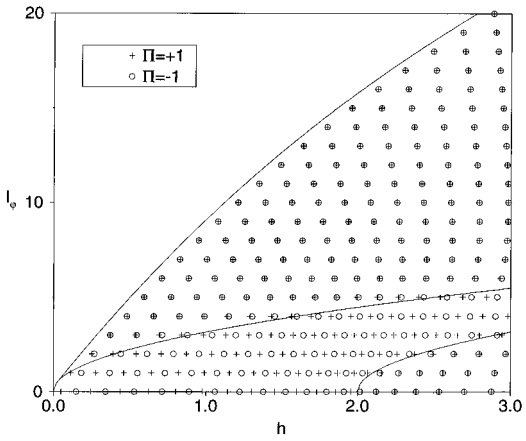

Figure 17. Same as Figure 16 except for $\theta = 0.05$. The upper part approximates the spectrum of the frameless spherical pendulum.

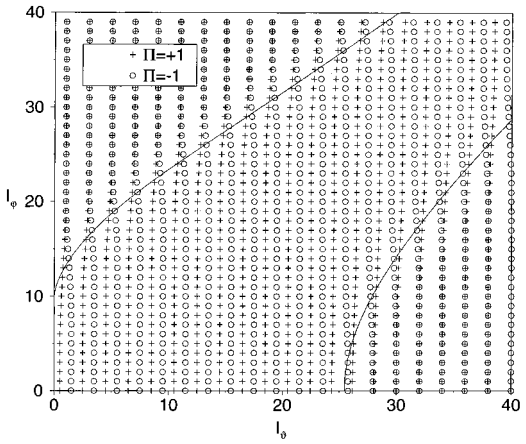

Figure 18. Spectrum of eq 42 for $\theta = 1$ and $\hbar = 0.1$, in action variable representation. The energy axis of Figure 16 has been transformed into the I_ϑ-axis by means of eq 26.

simply the even and odd real combinations of $e^{\pm ik\vartheta}$, with integer k and $2E_k = \hbar^2k^2$:

$$\psi_k^+(\vartheta) \propto \cos k\vartheta, \quad \psi_k^-(\vartheta) \propto \sin k\vartheta \tag{47}$$

In the intermediate region ${l_{s2}}^2 < {l_\varphi}^2 < {l_{s1}}^2$, the degeneracy is lifted; even and odd states alternate in energy. In the high-l_φ phase of spherical pendulum type motion, ${l_\varphi}^2 > {l_{s1}}^2 = 2\theta h$, even and odd states are again nearly—and in the limit $\theta \rightarrow 0$ completely—degenerate. The reason for this degeneracy is the infinitely high centrifugal potential $m^2\hbar^2/2 \sin^2 \vartheta$.

The regularities of the spectra become much more transparent if we transform them to the action variable representation, using the classical expression (26) to convert energy into I_ϑ. The result is shown in Figure 18, for the case $\theta = 1$. The picture is remarkably simple. Its basic pattern is a discretization with mesh sizes $\Delta I_\varphi = \Delta I_\vartheta = \hbar$, as was assumed in Bohr's old quantum theory. This is best seen in the intermediate phase where there is no spontaneous symmetry breaking, and hence no degeneracy. The degeneracies in the low- and high-l_φ phases imply a coalescence of eigenstates into pairs of equal actions, giving a mesh size $\Delta I_\vartheta = 2\hbar$ for the pairs. For a subset of states with given symmetry, this may be interpreted by saying that the effective shrinking of the available phase space volume by a factor ${}^1/_2$ is compensated by a factor 2 in the mesh size of actions.

There are only two features in the fine structure that the quantum theory of 1917 could not account for: one is the absolute position of the mesh, and the other is the transition

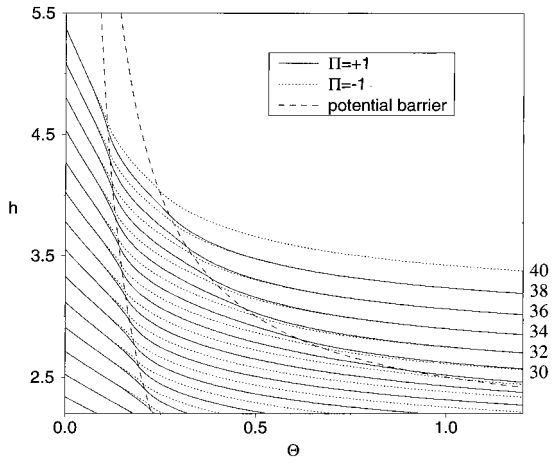

Figure 19. Variation of energy eigenvalues with θ, for $I_\varphi = 10\hbar$.

region near the classical separatrices. Both features do not affect the rule that there are nm states in a phase space volume of size $nm\hbar^2$; they only refer to the distribution of states within elementary cells.

The first feature can be dealt with in terms of Maslov indices, and is governed by a simple rule: action eigenvalues are $n\hbar$ for rotational motion along a 2π-circle, and $(n + {}^1/_2)\hbar$ for oscillatory motion.[20−22] This explains the details of Figure 18 except near the separatrices:

1. The φ-motion being always rotational, I_φ is everywhere $m\hbar$.

2. In the intermediate phase, $l_{s2}{}^2 < l_\varphi{}^2 < l_{s1}{}^2$, ϑ oscillates without degeneracy, hence $I_\vartheta = (n + {}^1/_2)\hbar$.

3. In the high-l_φ phase, $l_\varphi{}^2 > l_{s1}{}^2$, ϑ oscillates in either of the reduced phase spaces $\vartheta < \pi$ or $\vartheta > \pi$. This implies $I_\vartheta = (n + {}^1/_2)2\hbar$ for each of the two symmetry classes.

4. In the low-l_φ phase, $l_\varphi{}^2 < l_{s2}{}^2$, ϑ rotates in either of the reduced phase spaces $L_\vartheta > 0$ or $L_\vartheta < 0$. This implies $I_\vartheta = 2n\hbar$ for each of the two symmetry classes.

As to the behavior in the neighborhood of separatrices, the uniform quantization takes well care of it. To the extent that the potential can be approximated by $V(\vartheta) \approx V_0 - {}^1/_2\alpha(\vartheta - \vartheta_0)^2$ near a maximum at ϑ_0, the tunnel integral is on the order of $\pi\hbar$ or smaller for energies $|E - V_0| < \hbar\sqrt{\alpha}$. This gives an indication of the width of the transition region. For the potential (43) we find $\alpha = m^2\hbar^2/\theta^2 - 1$ at $\vartheta = \pi$, and $\alpha = m^2\hbar^2/\theta^2 + 1$ at $\vartheta = 0$. Transforming from energy to action I_ϑ this may be expressed as a "coherence length" for Maslov indices.

Let us now discuss the dependence of the spectrum on θ, for given angular momentum $I_\varphi = m\hbar$. Figure 19 shows energy eigenvalues with $m = 10$, for even states with 12, 14, ..., 38 nodes, and odd states with 14, 16, ..., 40 nodes (the number of nodes of a periodic function on a circle must be even). In the limit $\theta \to 0$, i.e., of two connected copies of frameless spherical pendulums, even states with n_ϑ nodes are strictly degenerate with odd states of $n_\vartheta + 2$ nodes. With increasing θ, the energy eigenvalues decrease, and a noticeable energy splitting between states $\psi^+(n_\vartheta)$ and $\psi^-(n_\vartheta + 2)$ takes place when the first separatrix is approached. Between the two separatrices, the levels keep almost equal distances in the order $\psi^+(n_\vartheta)$, $\psi^-(n_\vartheta + 2)$, $\psi^+(n_\vartheta + 2)$, ..., and for θ so high that the motion is dominated by the rotating pendulum type, states $\psi^+(n_\vartheta)$ and $\psi^-(n_\vartheta)$, with the same number of nodes, become degenerate.

How do these observations relate to the concept of spin that we introduced as a classical variable in eq 6? A quantum counterpart might be defined as the operator $\hat{\mathbf{s}}$,

$$\hat{\mathbf{s}}\psi(\vartheta) = \begin{cases} +\psi(\vartheta) & \text{if } 0 < \vartheta < \pi \\ -\psi(\vartheta) & \text{if } \pi < \vartheta < 2\pi \end{cases} \tag{48}$$

Notice that $\hat{\mathbf{s}}$ has expectation value 0 in any eigenstate of given parity,

$$\langle\psi^\pm|\hat{\mathbf{s}}|\psi^\pm\rangle = \oint \bar{\psi}^\pm(\vartheta)\,\hat{\mathbf{s}}\psi^\pm(\vartheta)\,\mathrm{d}\cos\vartheta = 0 \tag{49}$$

because of the minus sign introduced by $\hat{\mathbf{s}}$ in the range $\vartheta > \pi$. Nevertheless, in the limit $\theta \to 0$, the degenerate eigenstates of different parity may be recombined to give eigenstates of definite spin,

$$\psi^\uparrow = {}^1/_2(\psi^+(n_\vartheta) + \psi^-(n_\vartheta + 2)),$$
$$\psi^\downarrow = {}^1/_2(\psi^+(n_\vartheta) - \psi^-(n_\vartheta + 2)) \tag{50}$$

with

$$\hat{\mathbf{s}}\psi^\uparrow = \psi^\uparrow, \quad \hat{\mathbf{s}}\psi^\downarrow = -\psi^\downarrow \tag{51}$$

Under the influence of a frame with small nonzero θ, these spin eigenstates are no longer exact energy eigenstates. Instead, they are metastable states with lifetimes τ determined by the tunneling rate. The energy splitting between $\psi^+(n_\vartheta)$ and $\psi^-(n_\vartheta + 2)$ is of the order $\hbar/\tau$, in accordance with the uncertainty relation.

The situation is different if even and odd degenerate states in the low-l_φ phase are combined. In line with the physical nature of the corresponding classical tori $\mathcal{T}_{h,l_\varphi}$, there is no way to construct eigenstates of $\hat{\mathbf{s}}$ from these $\psi^+(n_\vartheta)$ and $\psi^-(n_\vartheta)$; the spin expectation value of such combinations remains zero because of the symmetry and orthogonality of the eigenstates.

6. Conclusion and Outlook

We have presented a coherent picture of the classical and quantum mechanics of a spherical pendulum suspended in a frame with vertical axis of rotation. The system is classically integrable, and we gave a full account of its phase space structure. The hyperelliptic nature of the problem, reflected in the presence of two separatrices, prevents analytic integration. But numerical computation allowed us to produce graphs providing comprehensive insight. We determined the bifurcation scheme of the energy-momentum mapping, the foliation of energy surfaces by invariant Liouville tori, and the representation of energy surfaces in terms of two action variables, $H = H(I_\varphi, I_\vartheta)$, from which we derived frequencies and winding ratios.

This representation is a convenient starting point not only for understanding but also for computing the quantum mechanical spectra. We used well established semiclassical methods to obtain results virtually identical to those of a straightforward solution of Schrödinger's equation. With a small set of additional rules, they are derived from a discretization of actions with mesh size $\hbar$.

Our main interest concerned the relationship of the spherical pendulum with frame to the pure, frameless spherical pendulum. The limit of vanishing moment of inertia θ of the frame cannot simply produce the textbook spherical pendulum, because the configuration space T^2 of the system with frame does not turn into a sphere S^2. However, we presented a scenario in which T^2 develops into two copies of S^2, and we suggest to view this as a possible classical concept of spin.

An analogous picture can be presented for the relationship of a rigid body suspended in a Cardan frame, with configuration space T^3, to the isolated rigid body whose configuration space is SO(3). As the moments of inertia of the frame tend to zero,

T^3 effectively develops into two copies of SO(3). This proposal is related to but different from the usual concept according to which spin is associated with the twofold covering of SO(3) by SU(2).

In a short deviation from the mainstream of the paper, we demonstrated that the spherical pendulum with frame can easily be made nonintegrable by giving the frame a tilt with respect to the vertical. The phase space structure is then considerably more complicated, and it will be interesting to study the quantum mechanics of this system. For small θ and tilt angles, perturbation theory may help to understand the nonchaotic regions, but on the whole, it will be necessary to perform extensive numerical calculations. The main challenge, we feel, is to invent pictures that would connect the results to those of the integrable limit.

References and Notes

(1) Born, M. *Vorlesungen über Atommechanik*; Springer: Berlin, 1925.

(2) Einstein, A. Zum Quantensatz von Sommerfeld und Epstein. *Verh. DPG* **1917**, *19*, 82−92.

(3) Berry, M. V. Some quantum-to-classical asymptotics. In *Chaos and Quantum Physics*; Giannoni et al., Eds.; Les Houches Summar School Lectures, Vol. 52; North Holland: Amsterdam, 1991; pp 251−303.

(4) Heller, E. J. Wave packet dynamics and quantum chaology. In *Chaos and Quantum Physics*; Les Houches Summer School Lectures, Vol. 52; North Holland: Amsterdam, 1991; pp 547−663.

(5) Gutzwiller, M. C. *Chaos in Classical and Quantum Mechanics*; Interdisciplinary Applied Mathematics; Springer: Berlin, 1990; Vol. 1.

(6) Berry, M. V. Regular and irregular motion. In *Topics in Nonlinear Dynamics*; AIP Conference Proceedings, No. 46; American Institute of Physics: New York, 1978; pp 16−120.

(7) Lichtenberg, A. J.; Lieberman, M. A. *Regular and Chaotic Dynamics*; Springer: Berlin, 1992.

(8) Richter, P. H. Die Theorie des Kreisels in Bildern. Report 226, Institut für Dynamische Systeme, 1990.

(9) Dullin, H. R. *Die Energieflächen des Kowalewskaja-Kreisels*; Mainz Verlag: Aachen, 1994; Dissertation.

(10) Dullin, H. R.; Juhnke, M.; Richter, P. H. Action integrals and energy surfaces of the Kovalevskaya top. *Bifurcation and Chaos* **1994**, *4*(6), 1535−1562.

(11) Richter, P. H.; Wittek, A.; Kharlamov, M. P.; Kharlamov, A. P. Action integrals for ellipsoidal billiards. *Z. Naturforsch.* **1995**, *50a*, 693−710.

(12) Wiersig, J.; Richter, P. H. Energy surfaces of ellipsoidal billiards. *Z. Naturforsch.* **1996**, *51a*, 219−241.

(13) Dullin, H. R.; Heudecker, O.; Juhnke, M.; Pleteit, H.; Schwebler, H.-P.; Waalkens, H.; Wiersig, J.; Wittek, A. Energy surfaces in action space; preprint, 1995.

(14) Richter, P. H.; Dullin, H. R.; Wittek, A. *Dynamics of the Spinning Top*; Springer Verlag: Berlin, in press.

(15) Bolsinov, A.; Dullin, H. R.; Wittek, A. Topology of energy surfaces and existence of transversal Poincaré sections. *J. Phys.* **1996**, *A29*, 4977−4985.

(16) Fomenko, A. T. Topological classification of all integrable Hamiltonian differential equations of general type with two degrees of freedom. In *The Geometry of Hamiltonian Systems*; T., Ratiu, Ed.; Springer: New York, 1991; pp 131−139.

(17) Oshemkov, A. A. Fomenko invariants for the main integrable cases of the rigid body motion equations. In *Topological Classification of Integrable Systems*; Fomenko, A. T., Ed.; American Mathematical Society: Providence, RI, 1991.

(18) Miller, W. H. Semiclassical treatment of multiple turning-point problems - phase shifts and eigenvalues. *J. Chem. Phys.* **1968**, *48*, 1651−1658.

(19) Child, M. S. Semiclassical theory of tunneling and curve-crossing problems: a diagrammatic approach. *J. Mol. Spectrosc.* **1974**, *53*, 280−301.

(20) Keller, J. B. Corrected Bohr-Sommerfeld quantum conditions for nonseparable systems. *Ann. Phys. (NY)* **1958**, *4*, 180−188.

(21) Maslov, V. P. *Théorie des Perturbations et Méthodes Asymptotiques*; Dunod: Paris, 1972.

(22) Percival, Ian C. Semiclassical theory of bound states. *Adv. Chem. Phys.* **1977**, *36*, 1−61.

JP9617128